Thermodynamic study of argon films adsorbed on boron nitride

A. D. Migone and M. T. Alkhafaji
Department of Physics and Molecular Science Program, Southern Illinois University, Carbondale, Illinois 62901

G. Vidali
Department of Physics, 201 Physics Building, Syracuse University, Syracuse, New York 13244-1130

M. Karimi*
Oak Ridge National Laboratory, Solid State Division, P.O. Box 2008, Oak Ridge, Tennessee 37831
(Received 10 August 1992)

We have performed a detailed adsorption isotherm study of Ar on BN for temperatures between 65 and 80 K. The isothermal compressibility of the films was obtained from adsorption data. At monolayer coverages, a small isotherm substep is present at melting. We found two isothermal compressibility peaks in the first layer: a sharp peak, corresponding to the melting substep, and a smaller, broader peak that occurs at lower pressures. At multilayer coverages we found reentrant layering occurring in the third and fourth layers of the film. We compare our layering results with predictions for the preroughening transition. We also found a series of small steps in the isotherms between the second and third layers and between the third and fourth layers of the film. These small steps are evidence of individual layer melting for the second and third layers. Our results at monolayer and at multilayer coverages are extensively compared to those found for Ar on graphite. We have also performed calculations of the rare-gas–BN interaction potentials. Our calculations indicate the substrate corrugation is smaller for the rare-gas–BN systems than it is for the same rare gases on graphite. The implications of this result for the possible existence of monolayer-commensurate solids on BN are discussed.

I. INTRODUCTION

Monolayer physisorbed films have been regarded for years as an important test ground for studies of matter in two dimensions (2D). Considerable work in experiment, simulation and theory has been devoted to determining the nature of monolayer phase transitions, particularly of melting.[1] This is largely the result of attempts to verify the unusual predictions of the Kosterlitz-Thouless-Nelson-Halperin-Young theory,[2] which states that melting can be a continuous transition in 2D. Experimentally, however, it has been found that the majority of 2D solids melt via first-order phase transitions.[3]

A wide range of phenomena in physical adsorption depend on the relative strengths of the adatom-adatom and adatom-substrate potentials, particularly for monolayer films.[4] Calculations for monolayers of Kr (Ref. 5) and Ar (Ref. 6) on graphite have shown that the amplitude of the periodic variation of the adatom-substrate potential energy across the substrate unit cell, i.e., the "substrate corrugation," has a strong influence on the solid phases found in these systems. The substrate corrugation is related to the strength of the Fourier component $V_{\mathbf{g}}$ ($\mathbf{g}$ is the 2D reciprocal-lattice vector of the substrate) of the adatom-substrate potential $V(r)$:

$$V(\mathbf{r})=V_0(z)+\sum_{\mathbf{g}\neq 0} V_{\mathbf{g}}(z)e^{i\mathbf{g}\cdot\mathbf{R}} , \tag{1}$$

where V_0 is the laterally averaged part of the potential, $\mathbf{r}$ is the vector pointing at the adsorbed atom, and $\mathbf{R}$ is its projection on the surface (the origin is at the surface). Simulations have shown that the adsorption potential needs to have large enough Fourier components, $V_{\mathbf{g}}$'s, if a commensurate phase is to be obtained.[5] For Kr on graphite,[5] substrate corrugation is responsible for the formation of a commensurate solid. For Ar on graphite, recent computer simulations[6] find that the effect of substrate corrugation is more subtle; it is responsible for the formation of a structure of commensurate patches separated by domain walls.

In recent years a growing emphasis in physisorption studies has been placed in multilayer films.[7] Initially, the focus was on wetting[8] and on the now disproved suggestion of using multilayer films to study surface melting.[9–12] It is now clear that few-layer films are interesting in their own right. Youn and Hess have recently discovered in an ellipsometric adsorption study of Ar on graphite a new phenomenon, called reentrant layering.[7,13] A reentrant layer is a layer which at low temperatures exhibits sharp adsorption isotherm steps; as the temperature is increased, a value is reached where the isotherm steps corresponding to this layer are no longer sharp (this is what occurs for a layer step measured above the layer critical point); at even higher temperatures, the layer steps become sharp again (this is the reentrant layering region). Above the reentrant layering temperature range, the layer steps are broad again. Youn and Hess found reentrant layering in the fourth, fifth, and sixth layers of Ar films but not in the three layers closest to the graphite substrate.[7,13] Currently there is no agreed upon explanation for this phenomenon, although it has been suggested that it might be a manifestation of a preroughening tran-

sition[14] in the Ar film.[15]

Experiments on physisorbed films have been performed mainly on graphite substrates. Increasingly, other high-quality substrates are currently utilized.[16–19] The availability of a variety of substrates allows the experimental determination of effects that different substrate symmetries and different values of substrate corrugation have on phases and transitions within adsorbed films. In the work reported here, boron nitride (BN) was used as substrate.

Hexagonal BN is isoelectronic to graphite.[20] The hexagons in BN are slightly larger than in graphite (the basal plane lattice parameter is 2.50 Å for BN and 2.46 Å for graphite).[21] The interlayer separation on BN is also comparable to that in graphite.

We report here on an investigation of Ar films on BN. We will present the following: (i) results of vapor pressure adsorption isotherms measurements at monolayer coverages to study the melting of Ar on BN; (ii) calculations conducted to determine the interaction potential between rare-gas atoms and the basal plane of BN and a discussion of the implications that these results have for the phase diagrams of rare gases on BN; and (iii) results of vapor pressure adsorption isotherms measured at multilayer coverages to study the reentrant layering behavior of multilayer Ar films. Preliminary reports of this work have appeared in two papers.[22,23] Here we present a comprehensive and detailed discussion of our results. Comparisons are made between our results for Ar on BN and previous experimental and theoretical work for Ar on graphite.

II. EXPERIMENTAL SETUP

The BN powder used in our measurements was manufactured by Union Carbide. It is commercially available as "HCP grade" BN. The reported specific area of this powder is 5 m^2/g. Since no structural studies have been performed on BN substrates, the monolayer capacity of the BN powder is less well defined than it is for a graphite substrate. In this study we have estimated the monolayer capacity from the lower end of the linear segment in the isotherm which exists between the beginning of the second-layer step and the small substep present in the first layer as measured on a 77.4-K Ar isotherm. This method probably yields an overestimate of monolayer capacity.

The BN samples used in most of our measurements were placed in a quartz tube and baked under a vacuum of 1×10^{-6} Torr at a maximum temperature of 770 K for an 8-h period. After the baking was completed, the powder was transferred in air from the quartz tube to the copper sample cell in which the experiments were made. The time of exposure to air of our powder sample was less than 20 min. We used different BN samples for the monolayer and multilayer studies.

In order to determine whether or not exposure of BN powder to air after baking affected the quality of the substrate, we performed for comparison measurements in which isotherms were determined on powder not exposed to air.[22] For this purpose we used a stainless-steel cell, which allowed us to take the powder from 770 to 77.4 K without breaking the vacuum integrity. After baking BN in this stainless-steel cell, we placed the cell inside a liquid-nitrogen container and performed an Ar adsorption isotherm. Our measurements were concentrated on a small substep (which is related to monolayer melting, as discussed below) that is present in the isotherm. This isotherm is shown in Fig. 1(a). After the isotherm was completed, the stainless-steel cell was brought to room temperature and the BN was exposed to air for approximately 1 h. The stainless-steel cell was then evacuated and placed inside liquid nitrogen. Another isotherm was performed on the air-exposed BN sample, the results are shown in Fig. 1(b). There is no measurable difference between the two isotherms, so we conclude that brief exposure to air after baking leaves the BN sample largely unaffected.[22]

Pressures were measured using 1000- and 10-Torr MKS Baratron gauges located in the dosing system, and they were corrected to account for thermal transpiration.[24] In a previous report[22] we had used an incorrect expression to account for this effect. This has led to some changes between the values presented here and those reported previously for data at monolayer coverages.

We have determined directly the temperature stability of our system by monitoring the value for the saturated vapor pressure of N_2 at 61.8 K over a period of 16 h. We find that the sample cell temperature remains constant to within ±0.003 K over this time period.

The quality of the BN substrate can be evaluated from the number of layer steps shown in multilayer adsorption

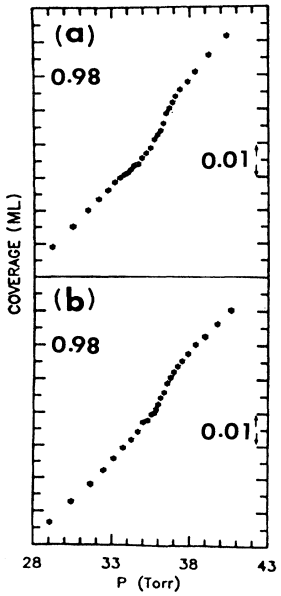

FIG. 1. Ar isotherms on BN measured at 77.4 K at coverages where a weak substep, signaling solidification of the film, is present in the data. Coverages are given in fractions of one layer (see text for definition of $n=1$). (a) Data measured on BN not exposed to air after baking. (b) Data measured on BN exposed to air. The arrows denote a coverage interval of 1% of a layer.

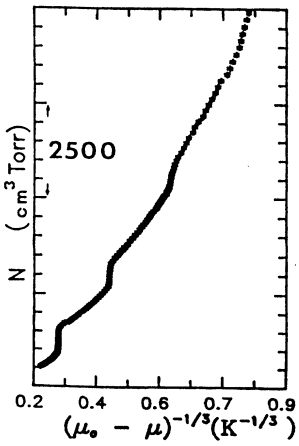

FIG. 2. Multilayer adsorption isotherm of Ar on BN at 66.93 K. The first layer is not shown in this data. The coverage is in units of cm^3 Torr. μ is the chemical potential of the film and μ_0 is the chemical potential corresponding to the bulk solid at the same temperature. The inverse cube power used in the x axis was chosen to separate more evenly the different layer steps. Steps for the second, third, fourth, and fifth layers are clear in the data.

data and from the sharpness of these steps. In Fig. 2 we display a 66.93-K multilayer adsorption isotherm (the data start above monolayer completion). Layer steps corresponding to the second, third, and fourth layers are clearly visible in the data, and a step corresponding to the fifth layer is resolvable. We have calculated the isothermal compressibility of the film from the adsorption data. The compressibility values for the 66.93-K isotherm are shown in Fig. 3. The height of the compressibility peaks (which correspond to the layer steps) are comparable to the values of the compressibility peaks determined for the layering steps of Kr on graphite.[25] This is the first time that isothermal compressibility data has been obtained for physisorbed films on a substrate other than graphite.

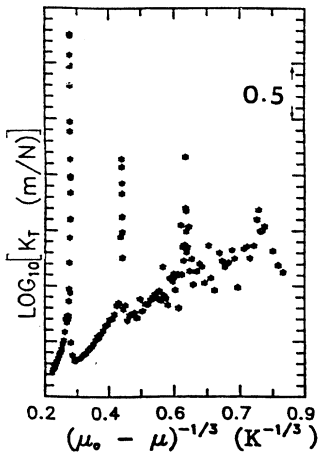

FIG. 3. Isothermal compressibility for the 66.93-K isotherm shown in Fig. 2. The compressibility is in units of m/N; its logarithm is plotted on the y axis. There is an isothermal compressibility peak corresponding to each layer step shown in Fig. 2. The largest isothermal compressibility peak shown corresponds to the second-layer step; as in Fig. 2, first-layer features are not shown.

III. CALCULATIONS OF THE RARE-GAS ATOMS–BN POTENTIALS

For the calculation of the rare-gas–BN potential we utilize a generalization of the method developed by Carlos and Cole,[26] which yielded an accurate helium-graphite potential using sums of carbon-helium Lennard-Jones potentials.[27] It was found that, in order to fit the data, it was necessary to take into account the anisotropy of the polarizability of the carbon atoms on the graphite basal plane. This method was later extended by Vidali and Cole[28] (VC) to other rare gases adsorbed on graphite. The principal effect of taking into account the anisotropy is an enhancement of the corrugation of the adatom-substrate potential. The use of the VC method in our calculations of rare-gas–BN potentials makes comparisons with results for graphite as meaningful as possible.

Following VC,[28] we write the gas-atom-surface potential energy as a sum of two-body anisotropic Lennard-Jones interactions $U(r)$:

$$\begin{aligned} V(\mathbf{r}) &= \sum_i U(\mathbf{r}-\mathbf{r}_i) , \\ U(\mathbf{x}) &= 4\epsilon\{(\sigma/x)^{12}[1+\gamma_r(1-\tfrac{6}{5}\cos^2\theta)] \\ &\quad -(\sigma/x)^6[1+\gamma_a(1-\tfrac{3}{2}\cos^2\theta)]\} , \end{aligned} \tag{2}$$

where ϵ and σ are the familiar Lennard-Jones energy and length parameters, $x=|\mathbf{x}|$, θ is the angle between $\mathbf{x}$ and the surface normal, and γ_a and γ_r are parameters associated with the anisotropy of the attractive and repulsive parts, respectively. The anisotropy affects only the Fourier components of the potential; the laterally averaged part reads

$$\begin{aligned} V_0(z) &= (4\pi\epsilon\sigma^6/A_s d^4)[\tfrac{2}{5}(\sigma/d)^6\zeta(10,z/d) \\ &\quad -\zeta(4,z/d)] , \\ \zeta(n,x) &= \sum_{\gamma=0}^{\infty}(j+x)^{-n} . \end{aligned} \tag{3}$$

For BN, $A_s=5.43$ Å^2 and $d=3.33$ Å, while for graphite $A_s=5.24$ Å^2 and $d=3.35$ Å.

The Lennard-Jones parameters were calculated using the method of the Chang and Crowell model.[29] Following Chang and Crowell,[29] the rare-gas–BN interaction was calculated as a sum of pairwise interactions between a rare-gas atom and an "effective" atom, $(BN)_{eff}$, at each hexagon vertex (i.e., in our calculation we do not distinguish between a B atom and a N atom). Considering the nature of the chemical bond and the similarities with graphite, this approximation should be acceptable.

The anisotropy in graphite arises because of the different values of the polarizability parallel or perpendic-

ular to the c axis. γ_a can be written as

$$\gamma_a = -\frac{2}{3}\frac{(1-b)}{(1+b)}, \quad b = \frac{P_\perp(1+E_a/E_\parallel)}{P_\parallel(1+E_a/E_\perp)}, \tag{4}$$

where $P_\perp$ and $P_\parallel$ are the substrate polarizabilities perpendicular and parallel to the c axis, respectively, $E_\parallel$ and $E_\perp$ are excitation energies for optical transitions in the substrate, and E_a is an excitation energy for the rare-gas atom. For rare-gas atoms interacting with graphite, $\gamma_a \approx 0.4$. γ_r controls the anisotropy of the repulsive part. For He-graphite, the value of $\gamma_r \sim -0.54$ was derived from He-graphite scattering data.[30] In this calculation we set $\gamma_r = 0$, since there are no sufficient data to guide our calculations for the systems considered here.

In order to determine the Lennard-Jones parameters for rare-gas–$(BN)_{eff}$ pair interaction, we used standard rules to combine parameters from rare-gas interactions with the ones of BN. Chang and Crowell obtained Lennard-Jones parameters by fitting to experimental values of interlayer spacing and Young's modulus. We followed a slightly different procedure. Since their work (1966), more reliable determinations have appeared in the literature for both rare-gas interaction parameters and rare-gas–BN adsorption energies. On the other hand, Young's modulus is poorly known. We took from the review article of Vidali *et al.*[31] the best determined ground-state energies for rare-gas–BN systems and used them to determine the Lennard-Jones parameters. Different rare-gas–BN systems gave slightly different values of Young's modulus. We took an average of these values and recalculated the Lennard-Jones parameters and ground-state energies. These latter values differ at most by 1% or 2% from the experimental ones. The new value of Young's modulus is 36% larger than the one used in Ref. 29.

To calculate γ_a for rare gases on BN, we first note that the electron band structures of BN and graphite have similarities, both having electrons in the π and σ states. Of course, there are significant differences as well: graphite is a semimetal, since the π bonding and antibonding bands intersect at the Fermi level, while BN is an insulator.

Because of symmetry rules, peaks in $\epsilon_\perp$ (the imaginary dielectric function polarized perpendicularly to the c axis) at about 6.5 and 14 eV can be related to $\pi \rightarrow \pi$ and $\sigma \rightarrow \sigma$ transitions. The characteristic energy $E_\perp$ is then $E_\perp = 0.25 \times 6.5$ eV $+ 0.75 \times 14$ eV ≈ 12 eV, where we supposed that roughly one electron in the π band and three electrons in the σ band contribute to the transition. The characteristic energy $E_\parallel$ is obtained by examining $\epsilon_\parallel$, which gives information on the $\pi \rightarrow \sigma$ transition (about 9.5 eV). The adatom excitation energy can be taken to be about the ionization energy (see Vidali and Cole[30] for a better determination). Except for helium, the average excitation energy can be taken to be 12–15 eV. To determine the ratio of polarizabilities R, $R = P_\perp/P_\parallel$, we follow the method that Phillips[32] used to estimate R for graphite. We find that R is about 2.5. With these values we obtain $\gamma_a \approx +0.3$. Because optical data for BN are not of the quality of those for graphite, the values of R and γ_a are more uncertain.

The results of our calculations are reported in Table I. $V_s - V_{sp}$ is the energy needed to go from the center of the BN hexagon to the saddle point (between the B and the N atoms). $V_s - V_{at}$ is the energy to go from the center of the BN hexagon to a site on top of the B or N atoms. Reported in Table II are values for the same quantities for adsorption of rare gases on graphite as evaluated by VC.[28] From an inspection of the tables, one can see that while there are only small differences between the well depths calculated on BN and graphite, the "activation" energies to move a rare-gas atom across the surface, both in absolute value and relative to the ground-state energy, are considerably smaller for the basal plane of BN than they are for the values for graphite. This result was somewhat surprising; naively, one expects the potential to be smoother for graphite, a semimetal, than for BN, an insulator. A calculation for Kr on BN using a different approach (Patrykiejew, Jaroniec, and Marczewski[33]) is in agreement with the trend found in our calculations.

The fact that for a given adatom the values of $V_s - V_{sp}$ and $V_s - V_{at}$ are smaller on BN than on graphite will be of importance in determining which solid phases can be exhibited by films of an adatom on these two substrates. Results from computer simulations for Kr on graphite[5] have found that in order to stabilize a commensurate solid layer, a sufficiently large substrate corrugation must

TABLE I. Results of calculations of the interaction between a rare-gas atom and the basal plane of BN. The subscripts s, sp, and at, indicate the adsorption site (center of the hexagon), bridge site (between B and N atoms), and atop site (on top of either B or N), respectively. V_0 is the minimum of the laterally averaged potential; z_0 is the position of the minimum of the laterally averaged potential; V_s, V_{sp}, and V_{at} are the values of the potential minima at the specified sites. NA indicates no anisotropy, i.e., $\gamma = 0$; AA indicates anisotropic attraction, i.e., $\gamma = 0.3$. σ and ϵ are the Lennard-Jones parameters for the interaction of a rare-gas atom with one atom of the substrate.

Atom	σ (Å)	ϵ (meV)	z_0 (Å)	V_0 (meV)	NA $V_{sp} - V_s$ (meV)	AA $V_{sp} - V_s$ (meV)	NA $V_{at} - V_s$ (meV)	AA $V_{at} - V_s$ (meV)
He	3.07	1.32	3.06	19.2	1.29	1.51	1.44	1.69
Ne	3.13	2.60	3.11	39.6	2.40	2.81	2.69	3.13
Ar	3.46	4.79	3.43	91.3	3.03	3.46	3.39	3.87
Kr	3.57	5.66	3.54	116.2	3.13	3.54	3.50	3.96
Xe	3.72	6.73	3.69	152.0	3.06	3.44	3.43	3.86

TABLE II. All symbols have the same meaning as in Table I except that here the substrate is the basal plane of graphite. For anisotropic attraction here $\gamma=0.4$. The results are taken from Ref. 28.

Atom	σ (Å)	ϵ (meV)	z_0 (Å)	V_0 (meV)	NA $V_{sp}-V_s$ (meV)	AA $V_{sp}-V_s$ (meV)	NA $V_{at}-V_s$ (meV)	AA $V_{at}-V_s$ (meV)
He	2.74	1.40	2.73	16.5	1.89	2.32	2.07	2.59
Ne	2.80	2.65	2.79	32.6	3.28	4.23	3.71	4.66
Ar	3.10	6.17	3.09	94.9	5.60	6.81	6.21	7.59
Kr	3.21	7.38	3.19	123.3	5.86	7.16	6.55	7.85
Xe	3.36	8.97	3.34	164.7	5.95	7.16	6.64	7.85

be used ($V_g \geq 0.6$ meV). Thus we expect that Kr should not be able to form commensurate phases on BN (recall that $V_s - V_{sp}$ is $\sim 8V_g$ and $V_s - V_{at}$ is $\sim 9V_g$).[28] This conjecture is in agreement with the results of adsorption experiments of Kr on BN,[19] which found no evidence for a commensurate-incommensurate transition in this system. It would be interesting to see whether computer simulations for Kr on BN agree with this speculation. Our results for the substrate corrugation also suggest that it would be of considerable interest to study on BN other adsorbates which form commensurate solids on graphite. The analysis of the situation for Ar films, which do not form a commensurate solid on graphite, is more complicated. The connection between the smaller corrugation in the substrate potential for Ar on BN relative to Ar on graphite and the possible melting mechanisms of Ar films on these two substrates are discussed in the next section.

IV. MONOLAYER RESULTS

In two previous studies of monolayer Ar films on BN, both adsorption isotherm as well as calorimetric adsorption measurements were performed.[34,35] Both studies found a very weak substep in the adsorption isotherm and a corresponding peak in the enthalpy of adsorption at the same coverage. These features were interpreted as signaling a freezing transition as the coverage increased. A broad peak in the enthalpy of adsorption occurring at coverages below freezing was also found in one of the studies; no interpretation was provided for this feature.[34]

Figure 4 shows four adsorption isotherms taken between 67.94 and 76.93 K. The only noticeable feature in the data is a small substep corresponding to a coverage change of no more than 1.5% of a layer. The pressures in Fig. 4 are scaled by the corresponding values of the pressure at the midpoint of the substep P_s. Following the analysis of previous studies,[34,35] we interpret this small substep as indicative of the solidification of the Ar film as coverage is increased. The small solidification step is displayed in greater detail in Fig. 1.

Our adsorption isotherm data are of sufficiently high quality to allow the calculation of the isothermal compressibility of the film. The expression for the two-dimensional isothermal compressibility K_T is

$$K_T = -(1/a)\frac{da}{d\phi} , \tag{5}$$

where a is the area per atom in the film ($a = A/N_f$, with A the total area of the substrate and N_f the number of atoms in the film) and ϕ is the spreading pressure of the film. The spreading pressure ϕ is not directly accessible to experiment. However, it is connected to measurable quantities by the equilibrium condition which holds on an isotherm: $ad\phi = vdP$. This expression relates the two-dimensional film and the three-dimensional vapor that coexists with it inside the sample cell; v is the specific volume of the three-dimensional vapor and P is its pressure. Substituting the equilibrium condition in Eq. (5) yields

$$K_T = -(1/n^2 v)\frac{dn}{dP} . \tag{6}$$

Here n is the two-dimensional film density ($n = N_f/A$).

Results for the isothermal compressibility of the 76.93-K isotherm are shown in Fig. 5. The isothermal compressibility is plotted versus the value of the chemical-potential difference between the film and the condensed bulk phase. Two features are clearly visible in the data: at higher values of the chemical potential there is a sharp peak (which corresponds to the small isotherm substep), and at lower values there is a broader, smaller peak.

To present our results more clearly, in Fig. 6 we plot

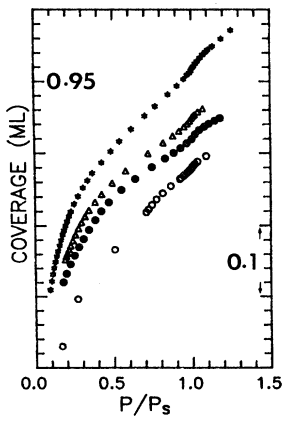

FIG. 4. Monolayer adsorption isotherms at four selected temperatures: open circles, 67.94 K; closed circles, 71.97 K; open triangles, 73.94 K; asterisks, 76.93 K. The pressures are scaled by the corresponding values of the pressure at the midpoint of the substep P_s. Arrows indicate a coverage interval of 10% of one layer.

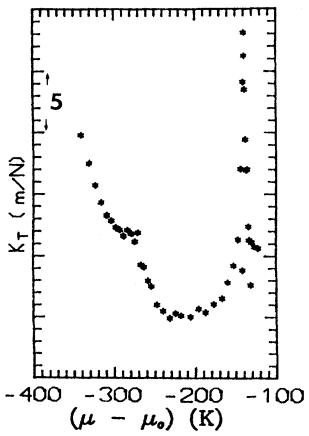

FIG. 5. Isothermal compressibility for the 76.93-K isotherm. The x axis gives the chemical-potential difference between the film and the condensed bulk solid phase. The sharp compressibility peak corresponds to the small isotherm substep.

the compressibility values obtained after subtraction of a smooth background contribution obtained by fitting the compressibility data away from the peaks to a polynomial. Two compressibility peaks are visible for all temperatures displayed. The sharp peak has a height of approximately 30±5 m/N and its shape and sharpness remain essentially unchanged with temperature. The broad peak is always smaller; it becomes sharper as the temperature is lowered. The separation between the two peaks in Fig. 6 increases as the temperature increases.[22]

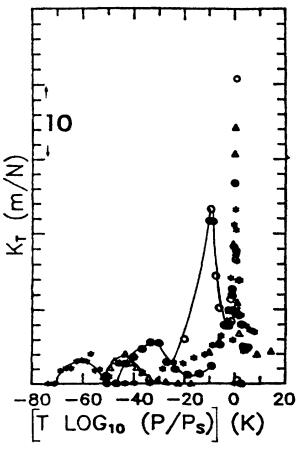

FIG. 6. Isothermal compressibility values obtained after subtracting a smooth background contribution from the data: 67.94 K (open circles), 71.97 K (closed circles), 73.94 K (open triangles), and 76.93 K (asterisks). Two compressibility peaks are visible for all temperatures displayed. The pressures are scaled by the respective values of the pressure at the midpoint of the substep P_s, so that the sharp compressibility peak feature overlaps for all the temperatures shown. The units for the x axis are the product of the isotherm temperature times the logarithm of the scaled pressure. The lines drawn through the data are guides to the eye.

In Fig. 7 we present the pressure P_s at the midpoint of the small monolayer substep plotted as a function of the inverse of the isotherm temperature. A least-squares fit to this data yields

$$\ln P_s = -(A/T) + B \ , \tag{7}$$

with $A = 1872.0$ K and $B = 27.773$; in Eq. (7) the pressure is expressed in Torr and the temperature in K. If the melting transition is first order, with solid and liquid phases coexisting on the surface, the intercept B has a simple interpretation provided that the substep occurs at constant coverage (this is not the case here, as can be seen in Fig. 4): B is proportional to the entropy difference between the coexisting film phases.[36]

If the coverage is fixed, Eq. (7) gives the isosteric heat of adsorption.[37] The low-coverage value of the isosteric heat of adsorption is directly related to the adatom-substrate binding energy. In our case the coverage is not fixed. However, since the coverage change is not large, the values for A and B are related to the film's isosteric heat and to the entropy difference between coexisting film phases, respectively.

The features of the isotherms and the isothermal compressibilities of Ar on BN (Ref. 22) are remarkably similar to those that have been found in a recent adsorption isotherm study of Ar on graphite:[38] (i) For Ar on graphite, there is a small substep at melting; the corresponding jump in this case is about 1.2% of a layer. (ii) The isothermal compressibility for Ar on graphite also exhibits two peaks, a broad small peak that occurs at coverages below freezing and a sharp melting peak of approximately 30 m/N in height. (iii) As is the case for Ar on BN, for Ar on graphite the smaller, broader peak appears to sharpen as the temperature is decreased. (iv) The temperature dependence of the pressure at the melting point is given by an equation of the same form as (7), with $A = 1955.4$ K and $B = 27.426$.[38] The value for B is very close to the $B = 27.773$ value found for Ar on BN.

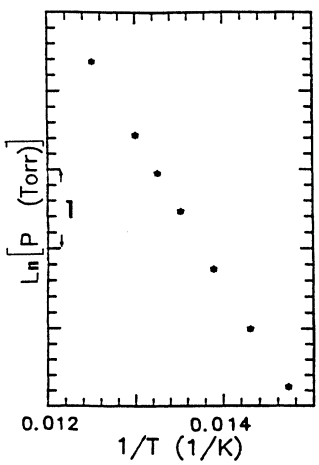

FIG. 7. The pressure at the midpoint of the small monolayer substep P_s plotted as a function of the inverse of the isotherm temperature.

There is only one qualitative difference in K_T found between these two systems: the separation between the location of the two isothermal compressibility peaks, expressed in terms of the units of Fig. 6, increases with increasing temperature for Ar on BN while it decreases with increasing temperature for Ar on graphite.[38] Since no computer simulations have been performed for Ar on BN, we can only speculate on the origins of this difference in behavior. It probably reflects differences in the corrugation in the respective adsorption potentials for these two systems.

In view of the high degree of similarity that exists between the melting data for Ar on graphite and Ar on BN, we will review some of the results for Ar on graphite in order to gain some insight. The recent isotherm study of Ar on graphite,[38] besides providing an important element of high-quality information on the Ar on graphite system with its compressibility results, has also virtually eliminated a longstanding controversy with its reanalysis of existing structural data. The controversy was centered on the presence or absence of a sharp feature in the data near the submonolayer melting transition for Ar on graphite: A first group of experimental studies [neutron scattering,[39] x rays,[40] low-energy electron diffraction (LEED),[41] calorimetry,[42] and adsorption isotherms[43]] found only broad, smooth features near monolayer melting for this system, suggestive of a possible continuous transition. Heat-capacity studies carried out in 1984 found for the first time a sharp but small heat-capacity peak associated with melting.[44] Approximately 3 K above the small, sharp heat-capacity peak there was a broader peak. The existence of any sharp features at melting was subsequently disputed in higher-resolution x-ray studies of this system.[45] The recent adsorption isotherm study[38] confirmed the existence of a sharp compressibility peak and a broader peak at lower coverages, both peaks occurring near the melting of monolayer Ar on graphite. Furthermore, in the isotherm study[38] the high-resolution x-ray data[45] were reanalyzed by calculating the temperature derivative of the correlation length of the solid determined by the x-ray measurements. The reanalysis showed that also the high-resolution x-ray data showed a sharp and broad feature associated with melting. This shows that for Ar on graphite all of the high-resolution data available, structural and thermodynamic, exhibit two features near melting; a broad one and a sharp one.

While the experimental results for Ar on graphite now appear free of disputes, disagreement remains regarding interpretations of the nature of the two peaks at melting and regarding the order of the melting transition for this system. The heat-capacity study[44] concluded that the sharp peak was associated with melting, that the transition was first order and that the higher-temperature broader peak was due to the gradual loss of order with increasing temperature on a liquid phase strongly influenced by the underlying substrate (as some computer simulations[46] seemed to indicate). Hence in this interpretation the broader peak did not imply the existence of a phase boundary. On the other hand, the isotherm results[38] were interpreted as indicating a continuous phase transition at the sharp isothermal compressibility peak. In this interpretation the melting involved a sequence of two steps, from the solid to a domain fluid phase characterized by small solidlike patches separated by domain walls; the solidlike domains transform into an isotropic fluid phase gradually, and this process is signalled by the broad compressibility peaks. Unfortunately, for the Ar on BN system (as is the case for Ar on graphite) it is impossible to determine experimentally without ambiguity whether the melting transition is weakly first order or continuous. It is likely, however, that the transition orders of both Ar on BN and Ar on graphite are the same.

Very recently, a computer-simulation study has been performed for Ar on graphite.[6] It was found that the substrate corrugation greatly influences the results. At temperatures below melting, the Ar monolayer forms patches in which the Ar atoms are in registry with the substrate; these patches are separated by domain walls. The domain walls form an ordered lattice at low temperatures. As the temperature is increased, the domain-wall lattice disorders; this disordering could appear in experiments as the sharp feature mentioned before. As the temperature is further increased, the domain-wall fluid rapidly evolves to a conventional fluid; this process might be responsible for the experimentally observed broad peak.[6] While the authors were unable to determine unequivocally the order of the transition from the simulations, they established that the transition could be at most weakly first order.

Because of the similarities in the isotherms and in the isothermal compressibilities, it is natural to suggest that the same alternative possible interpretations for the results which were put forth for Ar on graphite might apply for Ar on BN. In both explanations for the behavior of Ar on graphite, however, substrate corrugation is central. In one set of simulations[46] it is responsible for the liquid phase being nearly commensurate. In the other set of simulations, substrate corrugation is responsible for the formation of commensurate solid domains separated by domain walls.[6] We do not know whether the smaller substrate corrugation which we have found in our calculations for Ar on BN relative to Ar on graphite is large enough to produce either the nearly commensurate liquid of the Abraham simulations[46] or the domain-wall solid of the simulations of Shrimpton *et al.*,[6] both for Ar on graphite. The difference found for the values of the corrugation of the substrate potentials for Ar on BN and on graphite taken together with the considerable experimental similarities found between these two systems make Ar on BN a very intriguing system. It is a very interesting candidate for computer-simulation studies. Such studies should be able to provide considerable insight into the melting mechanism for Ar on BN as well as for Ar on graphite.

V. MULTILAYER RESULTS

The isotherms for the multilayer portion of this study start at coverages slightly above the monolayer melting transition and extend up to the fifth layer of the film. Iso-

therms were measured at 13 temperatures between 65 and 80 K.[23]

To examine the layering behavior of Ar films on BN, we present first our results for the temperature evolution of the second layer; this layer is not reentrant. In Fig. 8 we present portions of isotherms for coverages comprising the region of the second layer for temperatures between 66.93 and 79.91 K. At the lower temperatures a clear quasivertical step is present in the data. As the temperature increases, the steps become increasingly less vertical. The behavior of the second layer is in agreement with standard expectations for layering: the sharp layer steps end at a critical layering point, and for temperatures above this point only broad steps are present; there is no reentrant layering for the second layer. The observed behavior is also in agreement with the results for the second layer of Ar on graphite.[7,13]

In Fig. 9 we display third-layer isotherm steps for four representative temperatures. At 66.93 K the third-layer step is sharp. At 71.00 K the step is much broader and much less vertical. At 73.90 K the existence of a third layer is barely resolvable in the adsorption data. At 79.91 K, however, the third-layer step is once again clear and sharper than it is at either 71.00 or 73.90 K. Broad third-layer steps are observed between 71 and 77 K. The resharpening of the third layer begins at 77.96 K, and at 78.94 and 79.91 K the steps are quite sharp. From this we conclude that for Ar on BN the third layer exhibits reentrant layering. We note, however, that while the 78.94- and 79.91-K steps are sharp, they are not as sharp as those at 64.96 or 66.93 K. Third-layer reentrant layering has not been reported for Ar on graphite;[7,13] however, evidence for some degree of step resharpening in the third layer also exists in that case.[47]

A feature that is apparent in the data shown in Fig. 9 is that the sharp steps in the reentrant layering region (77.96, 78.94, and 79.91 K) occur at lower values of the coverage and chemical potential than those found in the low-temperature layering region. This behavior qualitatively agrees with what was found for the reentrant layering regime in the fourth, fifth, and sixth layers for Ar on graphite.[7,13] Capillary condensation can be seen in our isotherms in the fact that the isotherm portions between layer steps (i.e., the segments where there is considerable pressure change for relatively small coverage change) are not horizontal, and become increasingly less so as the coverage is increased, as can be seen in Fig. 2. Because of capillary condensation, we cannot unambiguously quantify how much lower the coverage of the reentrant steps is relative to the low-temperature sharp steps.

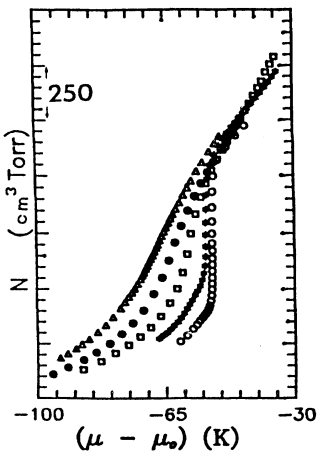

FIG. 8. Second-layer steps: 66.93 K (open circles), 69.93 K (asterisks), 73.90 K (open squares), 76.94 K (closed circles), and 79.91 K (open triangles). The chemical-potential difference is relative to the saturated bulk solid value μ_0. The coverage is in units of cm^3 Torr.

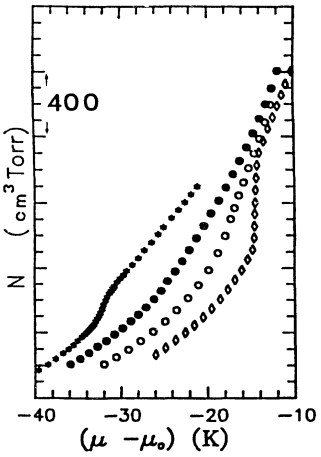

FIG. 9. Third-layer isotherm steps for four representative temperatures: 66.93 K (open rhombi), 71.00 K (open circles), 73.90 K (closed circles), and 79.91 K (asterisks). The third-layer step moves to lower chemical-potential values with increasing temperature. The 79.91-K step is reentrant: it is sharper than either the 71.00- or the 73.90-K step. The size of the step at 79.91 K is approximately $\frac{1}{2}$ the value of the step at 66.93 K.

The reentrant behavior of the third layer of the film is also clear in Fig. 10, which displays isothermal compressibilities for the third layer at seven temperatures. The results presented here were obtained from direct application of Eq. (6); no background contribution has been subtracted from these compressibility data. The values of the compressibilities measured at the different temperatures have been shifted along the y axis in order to display them more clearly. The high-temperature resharpening of the steps is quite evident in the compressibility data: the barely resolvable 73.90-K third layer has the broadest compressibility peak, while the peaks measured at 78.94 and 79.91 K are sharper than any of those measured between 71 and 77 K.

We have also found reentrant layering behavior in the fourth layer of the film. In Figs. 11 and 12, we show, respectively, isotherms and isothermal compressibilities for this layer. Qualitatively, the characteristics which we have found for the fourth layer of Ar on BN (Ref. 23) are the same as those seen for the fourth layer of Ar on graphite.[7,13] The temperature region in which the fourth-layer steps are broad is between 70 and 72 K. As is the case for the third layer, the reentrant layer appears

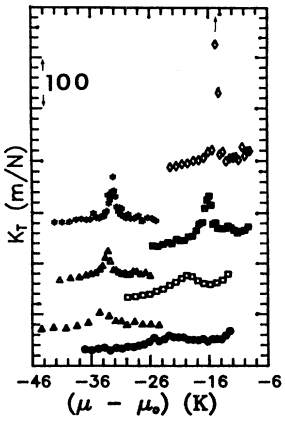

FIG. 10. Isothermal compressibilities for the third layer at seven temperatures: 66.93 K (open rhombi), 69.93 K (closed squares), 71.90 K (open squares), 73.90 K (closed circles), 77.96 K (closed triangles), 78.94 K (open triangles), and 79.91 K (asterisks). To avoid overlap between data at different temperatures, the peaks have been displaced along the y axis. The data show how the peaks move towards lower chemical potentials as a function of increasing temperature. The peak for 79.91 K is as sharp as that for 69.93 K, and sharper than for any other temperature between 71 and 78 K. The peak at 73.90 K is barely resolvable. The arrow for the 66.93 peak indicates points at higher values of the compressibility, which have been omitted for the sake of clarity.

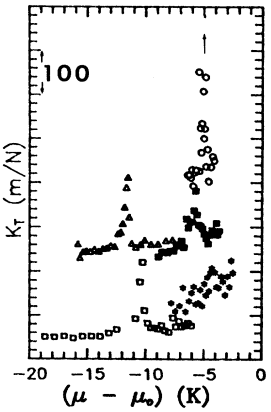

FIG. 12. Isothermal compressibilities for the fourth layer: 66.93 K (open circles), 68.98 K (closed squares), 69.93 K (asterisks), 73.90 K (open squares), and 78.94 K (open triangles). To avoid overlap between data at different temperatures, the peaks have been displaced along the y axis. The peak for 69.93 K is barely resolvable. The peaks at 73.90 and 78.94 K are sharper than that at 68.98 K. The arrow for the 66.93 peak indicates points at higher compressibility values, which have been omitted for the sake of clarity.

at lower values of the chemical potential and of the coverage. We should note that, as can be seen in Fig. 12, the compressibility peaks in the reentrant region, i.e., above 72 K, are as sharp as those seen below 70 K in the low-temperature sharp step region for this layer. This is different from what we observed for the third layer.

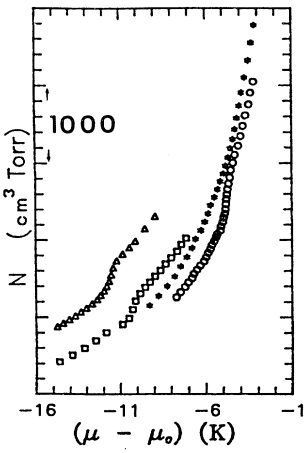

FIG. 11. Fourth-layer isotherm steps: 66.93 K (open circles), 69.93 K (asterisks), 73.90 K (open squares), and 78.94 K (open triangles). The step moves to lower chemical potentials with increasing temperatures. At 69.93 K the fourth layer is virtually unresolvable. The height of the reentrant step at 73.90 K is approximately $\frac{1}{2}$ that at 66.93 K.

A characteristic shared by the reentrant layering steps for the third and fourth layers is that when they first appear, at 78.94 K for the third layer and at 72.95 K for the fourth layer, the step height for the reentrant layer is smaller than the height of the layer in the lower-temperature sharp step region. In Figs. 9 and 11 the third and fourth reentrant layers are approximately one half the size of the corresponding low-temperature sharp layering values. The same behavior was also observed for the fourth layer of Ar on graphite in the ellipsometric study.[7] Both on graphite and on BN, the size of the reentrant fourth layer step increases for higher temperatures.

The possibility that the reentrant layering observed for Ar on graphite was a manifestation of a preroughening transition taking place in the Ar film was suggested by den Nijs.[15] Preroughening is a phase transition which occurs on crystal surfaces and is signaled by the appearance of a new type of phase, the disordered flat phase.[14,15]

In the more traditional roughening scenario, a crystalline surface is flat at low temperatures; as the roughening transition temperature is approached, the free energy required for forming a step on the surface of the crystal vanishes, and as a result the surface goes from being flat to having steps and forming a terraced mountain landscape. This is called the rough phase. In the preroughening picture a new phase, of characteristics intermediate between the flat and the rough, appears; it is the disordered flat phase. In the disordered flat phase the surface of the crystal on average remains flat, although it contains a disordered array of steps.[14] Up and down steps alternate. The average height in the disordered flat phase is shifted by $\frac{1}{2}$ relative to the ordered flat phase. An essential feature of a multilayer film undergoing

preroughening is a $\frac{1}{2}$ layer shift in the average height of the top layer.[15]

The question of whether the preroughening scenario is the explanation for reentrant layering is still open. Some of our results for Ar on BN offer support for an interpretation of reentrant layering in terms of preroughening. At the temperature at which a reentrant layer just appears, the height of the layer is $\frac{1}{2}$ the height of the value of the layer at low temperatures. Since preroughening is a transition occurring on the face of the crystal, the appearance of this transition in an adsorbed film should be independent of the substrate used.[15] The similarity in the behavior observed for Ar on BN and on graphite suggests that this is the case. In a previous paper[23] we had argued that the fact that we observed reentrant layering in the third layer was an argument against a preroughening interpretation. This is not necessarily the case; after the first two layers, the Ar atoms must already know that they prefer the *ABC* packing instead of *ABA*; so, two layers are enough for reentrant growth.[48] The onset of preroughening can vary on different substrates.[48] On the other hand, den Nijs has noted that the suggestion that the (111) facet of a Lennard-Jones-type solid preroughens is surprising, because it implies the existence of an as-yet-unknown reconstructed state, energetically quite close to the flat phase, which plays a role of parent state for the disordered flat phase.[15]

In addition to layering steps, which are easily identified as such by the large coverage changes involved in them, we can also identify in the isotherms a series of smaller substeps. These small steps are observed at coverages intermediate between the second and third layers and between the third and fourth layers, and we associate them with melting transitions for the individual layers.[23]

The existence of individual layer-by-layer melting behavior has been well documented in Ar on graphite. Evidence for individual layer-by-layer melting for the second and third layers of the Ar film has been seen in heat-capacity studies by Zhu and Dash[9] (while the higher coverages investigated in this study are significantly affected by capillary condensation, results at the lower coverages are substantially free from this effect). Individual heat-capacity peaks identified with melting of the second and third layers of the film were measured.[9] Neutron-scattering studies by Larese and Zhang[11] performed on bilayer and trilayer films have shown directly the layer-by-layer nature of the melting. This study showed that the number of solid layers decreases in layer-by-layer fashion with increasing temperature, while at the same time the number of liquid layers increases, also in layer-by-layer fashion.[11] Computer simulations by Phillips[49] and Cheng and Steele[5] have also found this layer-by-layer melting behavior.

The existence of a sequence of layer-by-layer melting transitions forming a zig-zag line between the third, fourth, fifth, and sixth layers, interconnecting the observed reentrant layering transitions, was suggested in the ellipsometric study of Ar on graphite.[7,13] The corresponding features were not detected in the isotherms, presumably because the density change involved in melting is relatively too small to be observed with this technique.

In Fig. 13 we display portions of isotherms at 71.00 and 73.90 K in the region of second-layer melting. The corresponding isothermal compressibilities are shown in Fig. 14. The data are qualitatively similar to the bilayer heat-capacity melting data. In the heat-capacity data there is first a cusp at lower temperatures followed by a gradual drop at higher temperatures. In the data shown in Fig. 14 there is a gradual rise to a peak at lower pressures followed by a sharp drop at higher pressures. The sharp features appear in reverse order in isotherm and heat-capacity experiments because in the heat capacity the solid phase is present at low temperatures and in the adsorption measurements it appears at high pressures, as was noted in Ref. 38.

Even if no first-order discontinuity appears to be present in either the isotherm data or in the compressibil-

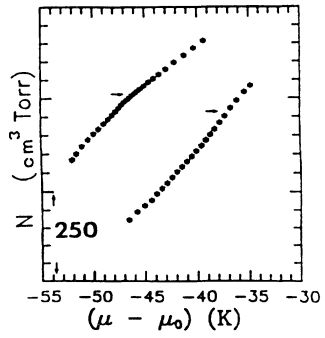

FIG. 13. Second-layer melting at 71.00 K (left) and 73.90 K (right). For the 71.00-K isotherm near the melting region, the data points are space data intervals closer than 1% of a layer.

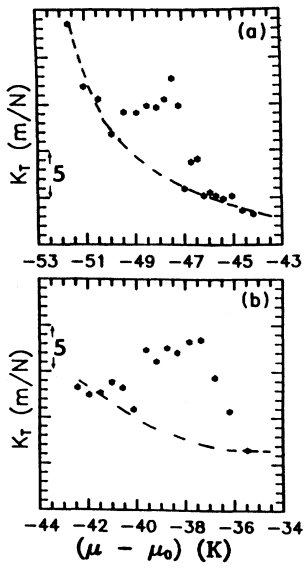

FIG. 14. Isothermal compressibilities corresponding to the bilayer melting data for the (a) 71.00-K and (b) 73.90-K isotherms. The dashed line is a guide to the eye, showing a smooth background compressibility.

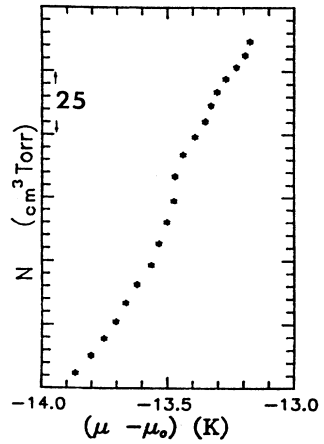

FIG. 15. Isotherm data corresponding to the third-layer melting region at 69.93 K. Note the narrow intervals in coverage and in chemical potential used in order to measure this substep.

ity, it is very difficult to extract the order of the bilayer melting transition. Both the simulations by Phillips[49] and those by Cheng and Steele[50] have found that layer promotion takes place on Ar on graphite prior to melting. Cheng and Steele[50] have pointed out that in these circumstances melting cannot proceed at constant spreading pressure and, hence, melting signatures would not appear sharp even if the process were first order.

In Fig. 15 we display isotherm data corresponding to the third-layer melting region at 69.93 K. Note that a rather small chemical-potential interval is covered to observe this transition. For the melting of the third layer there is evidence in the computer-simulation studies of even greater layer promotion[49,50] occurring than for the second layer, so the cautionary note regarding the determination of the order of the transition applies even more strongly here.

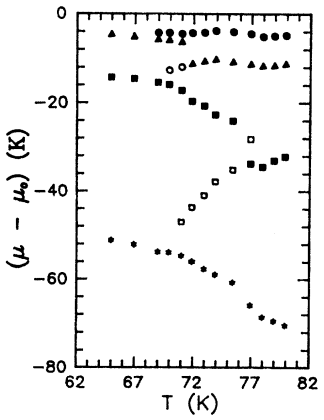

FIG. 16. Chemical potential vs temperature phase diagram for the multilayer region of Ar on BN. Open symbols are used for melting transitions, and closed symbols are used for layering transitions. Asterisks mark the location of second-layer steps; closed squares, third-layer steps; closed triangles, fourth-layer steps; and closed circles, fifth-layer steps. The broad layering isotherm steps occur in the regions with large negative slope while the sharp steps occur for regions with near-zero slope.

In Fig. 16 we present a chemical potential versus temperature phase diagram for the multilayer region of Ar on BN which encompasses all of our results at once. This diagram is very similar to that found for Ar on graphite.[7,13] Indeed, the multilayer phase diagrams of Ar, Kr, and Xe starting from the second layer up are quite similar to each other,[7] in clear distinction to what occurs with their respective monolayer phase diagrams, which are all different. This is a result of the decreasing influence of the substrate in layers above the first.

VI. CONCLUSION

The results of the adsorption studies presented here for Ar films on BN clearly show BN to be a very-high-quality substrate. The degree of substrate homogeneity is attested to by the number of isotherm steps that can be resolved as well as by the sharpness of these steps in the low-temperature layering regime. While BN cannot be used as substrate in neutron-scattering measurements because of the large cross section for B atoms, BN may offer some advantages over graphite with other techniques, such as NMR, because it is an insulator.

Our calculations for the rare-gases–BN interaction potential indicate that the substrate corrugation is smaller for these systems than for the same gases on graphite. The calculation indicates that the strength of the corrugation is too small to form a commensurate solid phase for Kr (which is indeed not observed experimentally). Because of these differences, detailed experiments and simulations on adsorbates on BN which form commensurate solids on graphite should yield quite interesting results.

We have found that a great deal of similarity exists between the Ar on graphite and the Ar on BN systems, both at monolayer and at multilayer coverages. Monolayer melting of Ar on BN shares a large number of characteristics with monolayer melting on graphite. Unfortunately, in neither case is it possible to determine experimentally without ambiguity the order of the monolayer melting transition; in both cases it is either weakly first order or continuous. The observed similarities at melting of Ar on these two substrates is somewhat surprising in view of the difference which we have found between their corresponding substrate corrugations. Computer-simulation studies for the melting of Ar on BN should prove to be quite illuminating in this regard.

At multilayer coverages we found reentrant layering in the third and in the fourth layers of the film. While our results lend some support to a preroughening explanation for reentrant layering, the nature of this phenomenon remains still unresolved. We have found evidence for layer-by-layer melting in this system for the second and third layers of the film, a result in agreement with what was found for Ar on graphite.

ACKNOWLEDGMENTS

The authors thank M. den Nijs for illuminating comments on the preroughening transition. The authors would also like to thank J. M. Phillips, W. A. Steele, J. Z. Larese, and D. M. Zhu for helpful discussions. One of us (A.D.M.) would like to acknowledge support for this research by the National Science Foundation through Grant No. DMR-9242404 and by the Materials Technology Center of Southern Illinois University. Another one of us (G.V.) would like to acknowledge support from NASA, Astrophysics Division.

*Permanent Address: Department of Physics, Indiana University of Pennsylvania, Indiana, PA 15705.

[1]For a recent review of monolayer phase diagrams see M. H. W. Chan, in *Phase Transitions in Surface Films 2,* Vol. 267 of *NATO Advanced Study Institute, Series B: Physics,* edited by H. Taub, G. Torzo, H. J. Lauter, and S. C. Fain, Jr. (Plenum, New York, 1991), p. 1.

[2]J. M. Kosterlitz and D. J. Thouless, J. Phys. C **6**, 1181 (1973); D. R. Nelson and B. I. Halperin, Phys. Rev. B **19**, 2457 (1979); A. P. Young, *ibid.* **19**, 1855 (1979).

[3]This topic has been reviewed by K. J. Strandburg, Rev. Mod. Phys. **60**, 161 (1988).

[4]L. W. Bruch, in *Phase Transitions in Surface Films 2* (Ref. 1), p. 67.

[5]N. D. Shrimpton, B. Joos, and B. Bergersen, Phys. Rev. B **38**, 2124 (1988).

[6]N. D. Shrimpton, H. Y. Kim, W. A. Steele, and A. Cheng (unpublished).

[7]G. B. Hess, in *Phase Transitions in Surface Films 2* (Ref. 1), p. 357, and references cited therein.

[8]R. Pandit, M. Schick, and M. Wortis, Phys. Rev. B **26**, 5112 (1982).

[9]D. M. Zhu and J. G. Dash, Phys. Rev. Lett. **57**, 2959 (1986); Phys. Rev. B **38**, 11 673 (1988).

[10]J. Z. Larese, Q. M. Zhang, L. Passell, J. M. Hastings, J. R. Dennison, and H. Taub, Phys. Rev. B **40**, 4271 (1989).

[11]J. Z. Larese and Q. M. Zhang, Phys. Rev. Lett. **64**, 922 (1990).

[12]J. M. Gay, J. Suzanne, J. G. Dash, and H. J. Lauter, J. Phys. I France **1**, 1279 (1991).

[13]H. S. Youn and G. B. Hess, Phys. Rev. Lett. **64**, 918 (1990).

[14]K. Rommelse and M. den Nijs, Phys. Rev. Lett. **59**, 2578 (1987); M. den Nijs, *ibid.* **64**, 453 (1990).

[15]M. den Nijs, Phys. Rev. Lett. **66**, 907 (1991); *Phase Transitions in Surface Films 2* (Ref. 1), p. 247.

[16]J. Ma, D. L. Kingsbury, F. C. Liu, and O. E. Vilches, Phys. Rev. Lett. **61**, 2346 (1988); J. P. Coulomb, T. S. Sullivan, and O. E. Vilches, Phys. Rev. B **30**, 4753 (1984); J. P. Coulomb and O. E. Vilches, J. Phys. (Paris) **45**, 1381 (1984).

[17]T. W. Kenny and P. M. Richards, Rev. Sci. Instrum. **61**, 822 (1990).

[18]F. Millot, Y. Larher, and C. Tessier, J. Chem. Phys. **76**, 3327 (1982).

[19]N. Dupont-Pavlovsky, C. Bockel, and A. Thomy, Surf. Sci. **160**, 12 (1985).

[20]A. Catellani, M. Posternak, A. Baldereschi, H. J. F. Jansen, and A. J. Freeman, Phys. Rev. B **32**, 6997 (1985); J. Robertson, *ibid.* **29**, 2131 (1983).

[21]R. W. G. Wyckoff, *Crystal Structures,* 2nd ed. (Interscience, New York, 1963).

[22]M. T. Alkhafaji and A. D. Migone, Phys. Rev. B **43**, 8741 (1991).

[23]M. T. Alkhafaji and A. D. Migone, Phys. Rev. B **45**, 8767 (1992).

[24]T. Takaishi and Y. Sensui, Trans. Faraday Soc. **59**, 2503 (1963).

[25]R. Gangwar and R. M. Suter, Phys. Rev. B **42**, 2711 (1990).

[26]W. E. Carlos and M. W. Cole, Surf. Sci. **91**, 339 (1980).

[27]W. A. Steele, *The Interaction of Gases with Solid Surfaces* (Pergamon, Oxford, 1974).

[28]G. Vidali and M. W. Cole, Phys. Rev. B **29**, 6736 (1984).

[29]A. D. Crowell and C. O. Chang, J. Chem. Phys. **43**, 4364 (1965).

[30]G. Vidali and M. W. Cole, Surf. Sci. **110**, 10 (1981).

[31]G. Vidali, G. Ihm, H.-Y. Kim, and M. W. Cole, Surf. Sci. Rep. **12**, 133 (1991).

[32]J. C. Phillips, *Covalent Bonding in Crystals, Molecules and Polymers* (Chicago University Press, Chicago, 1969).

[33]A. Patrykiejew, M. Jaroniec, and A. M. Marczewski, Chem. Scipta **22**, 136 (1983).

[34]Y. Grillet and J. Rouquerol, J. Colloid Interface Sci. **77**, 580 (1980).

[35]F. Rodriguez-Reinoso, J. de D. Lopez-Gonzalez, I. Bautista, Y. Grillet, F. Rouquerol, and J. Rouquerol, in *Adsorption at the Gas-Solid Interface,* edited by J. Rouquerol (Elsevier, Amsterdam, 1982).

[36]Y. Lahrer, J. Chim, Phys. **65**, 974 (1968).

[37]J. G. Dash, *Films on Solid Surfaces* (Academic, London, 1975).

[38]Q. M. Zhang and J. Z. Larese, Phys. Rev. B **43**, 938 (1991).

[39]H. Taub, K. Carneiro, J. K. Kjems, L. Passell, and J. P. McTague, Phys. Rev. B **16**, 2457 (1979).

[40]J. P. McTague, J. Als-Nielsen, J. Bohr, and M. Nielsen, Phys. Rev. B **25**, 7765 (1982).

[41]C. G. Shaw, S. C. Fain, Jr., and M. D. Chinn, Phys. Rev. Lett. **41**, 955 (1978).

[42]T. T. Chung, Surf. Sci. **87**, 438 (1979).

[43]Y. Lahrer, Surf. Sci. **134**, 438 (1979).

[44]A. D. Migone, Z. R. Li, and M. H. W. Chan, Phys. Rev. Lett. **53**, 810 (1984).

[45]M. Nielsen, J. Als-Nielsen, J. Bohr, J. P. McTague, D. E. Moncton, and P. W. Stephens, Phys. Rev. B **35**, 1419 (1987); K. L. D'Amico, J. Bohr, D. E. Moncton, and Doon Gibbs, *ibid.* **41**, 4368 (1990).

[46]F. F. Abraham, Phys. Rev. B **28**, 7338 (1983).

[47]G. B. Hess (private communication).

[48]M. den Nijs (private communication).

[49]J. M. Phillips, Phys. Lett. A **147**, 54 (1990).

[50]A. L. Cheng and W. A. Steele, Langmuir **5**, 600 (1989).